Geophysical Research Letters

RESEARCH LETTER
10.1029/2025GL118931

Solar Orbiter Observations of a Self-Consistent Ion-Scale Magnetic Hole at 0.9AU

Jing-Huan Li[1], Yuri V. Khotyaintsev[1], Daniel B. Graham[1], Timothy Horbury[2], and Philippe Louarn[3]

[1]Swedish Institute of Space Physics, Uppsala, Sweden, [2]Imperial College London, London, UK, [3]Institut de Recherche en Astrophysique et Planétologie, CNES-CNRS Universite Toulouse III Paul Sabatier, Toulouse, France

Key Points:

- Solar Orbiter observed a self-consistent ion-scale magnetic hole (MH) in the solar wind
- The deep MH, with a minimum magnetic field of 0.15 nT, leads to quasi-isotropic ion pitch-angle distributions
- We use a kinetic equilibrium model to reconstruct the MH, and the results agree well with the observations

Correspondence to:
J.-H. Li,
jinghuan.li@irfu.se

Citation:
Li, J.-H., Khotyaintsev, Y. V., Graham, D. B., Horbury, T., & Louarn, P. (2025). Solar orbiter observations of a self-consistent ion-scale magnetic hole at 0.9AU. *Geophysical Research Letters*, *52*, e2025GL118931. https://doi.org/10.1029/2025GL118931

Received 18 AUG 2025
Accepted 6 NOV 2025

Abstract Magnetic holes (MHs) are localized structures characterized by magnetic field depressions, accompanied by an enhancement in plasma thermal pressure. These pressure-balanced structures span a broad range of scales in space, from fluid to kinetic regimes. The kinetic-scale MHs are ubiquitous in the solar wind; however, the exploration is limited due to the lack of high-resolution particle measurements. Here, we utilize Solar Orbiter observations to explore ion dynamics within an ion-scale MH. The ion energy spectrum exhibits enhanced and depressed phase-space densities for ions above and below 10 eV, respectively. The enhancements of perpendicular and parallel temperatures in this deep MH result in a quasi-isotropic ion pitch angle distribution. The ion diamagnetic drift contributes to the agyrotropy around the boundaries, forming an ion vortex consistent with the magnetic field depression. These results align well with a kinetic equilibrium model, confirming the stability and self-consistency of ion-scale MHs in the solar wind.

Plain Language Summary Localized depressions in the magnetic field strength have been observed by the satellites in various plasma environments. They are identified as linear magnetic holes or cavities owing to the negligible variation in magnetic field direction. They are pressure-balanced structures with increased plasma density and/or temperature. In the solar wind, because of the strong convection, the ion-scale magnetic holes (MHs) are typically observed for only ∼10 s, making it challenging to resolve the associated ion dynamics. Using high-resolution Solar Orbiter observations, we investigate a deep ion-scale magnetic hole with a minimum strength of 0.15 nT. Within this structure, the decrease in phase-space densities (PSDs) for ions with energies below 10 eV is accompanied by an enhancement in PSDs for ions with energies above 10 eV, indicative of a temperature increase. Notably, the temperature rises simultaneously in both directions perpendicular and parallel to the magnetic field, and the ion velocity distributions become nearly isotropic at the center. This is different from the usual pancake distributions observed in the terrestrial magnetosheath. Finally, a kinetic equilibrium model can well reproduce these observational signatures, suggesting that the self-consistent ion-scale MH is stable in the solar wind.

1. Introduction

Magnetic holes (MHs) are quasi-symmetric structures characterized by a localized depression in magnetic field strength and a corresponding enhancement in plasma density and temperature (Shi et al., 2024; Yao et al., 2021). These pressure-balanced structures span a broad range of spatial scales, from magnetohydrodynamic (MHD) to electron scales. They are observed ubiquitously in space plasmas, including the solar wind (Turner et al., 1977; Xiao et al., 2010), terrestrial (Goodrich et al., 2016; Huang et al., 2022; Zhang et al., 2017), planetary (Cattaneo et al., 1998; Goodrich et al., 2021; Huang et al., 2021; Joy et al., 2006), and cometary environments (Plaschke et al., 2018; Russell et al., 1987). MHs frequently appear in conjunction with other fundamental phenomena, such as turbulence (Haynes et al., 2015), magnetic reconnection (Wang et al., 2024), shocks (Karlsson et al., 2022; Yao et al., 2024), dipolarization fronts (C. Liu et al., 2021), and current sheets (G. Wang et al., 2022).

For MHs at sub-ion scales (i.e., spatial extents smaller than the thermal proton gyroradius, ρ_i), significant progress has been made in understanding corresponding electron dynamics, largely owing to high-resolution observations from NASA's Magnetospheric Multiscale (MMS) mission. Such MHs primarily trap pitch angle ∼90° electrons, generating diamagnetic currents that support the observed magnetic field depressions (Yao et al., 2017). The resulting pancake electron distributions give rise to temperature anisotropies ($T_\perp > T_\parallel$), which can consequently excite whistler-mode waves (Yao et al., 2019). Moreover, the electrostatic waves observed inside the sub-ion

scale MHs, such as solitary waves and electron cyclotron waves, are associated with the electron beams (Yao et al., 2019). These structures, convected by the ambient plasma flow (Yao et al., 2016), have quasi-circular cross-sections in the plane perpendicular to the background magnetic field (Liu, Zong, Zhang, Xiao, et al., 2019). Though their formation mechanisms remain debated (Shi et al., 2024), most properties of sub-ion scale MHs have been clarified through in situ measurements (Yao et al., 2017), particle-in-cell simulations (Haynes et al., 2015), and kinetic equilibrium models (Li, Zhou, Yang, et al., 2021; Li et al., 2020).

In contrast, the understanding of ion-scale MHs, structures with spatial scales exceeding ρ_i, is still limited. MMS has reported that ion-scale MHs in the magnetosheath are supported by ion vortices (Yao et al., 2023), analogous in structure to electron-vortex MHs. The ion vortex can sometimes embed another electron vortex, where electron and ion thermal pressures are enhanced, respectively, to maintain pressure balance for corresponding structures (Liu, Zong, Zhang, Xiao, et al., 2019). Additionally, the ion-vortex MH can have a reversed field direction at the center, indicating its complex evolution processes (Yao et al., 2023). These ion-scale structures are accompanied by complicated electron pitch angle distributions (Li, Zhou, Zong, et al., 2021; Yao et al., 2018), which can consequently drive various plasma waves (Boldú et al., 2023; Yao et al., 2023). Thus, ion-scale MHs can impact the generation of vortices and waves at electron scales, playing a role in the turbulent energy cascade and dissipation.

A typical turbulent plasma environment is the solar wind, where MHs are routinely observed by numerous spacecraft from 0.166 AU to beyond 17 AU (Russell et al., 2008; Sperveslage et al., 2000; Yu et al., 2021). The isolated MHs may represent remnants of the mirror-mode structures (Winterhalter et al., 1994), which are occasionally observed as extended trains referred to as mirror-mode storms (Dimmock et al., 2022). As for the ion-scale MHs, they are known to be frozen into plasma and convected by the background solar wind flow (Trollvik et al., 2023). MMS observations have further revealed the presence of an ion vortex associated with such structures (Wang et al., 2021). However, since the MMS spacecraft are optimized for measurements in slow-moving and high-temperature plasmas, their particle data in the solar wind typically overestimate ion temperatures and underestimate densities (Roberts et al., 2021; Wilson et al., 2022). As a result, although MMS data have high temporal resolution, detailed investigations of ion dynamics within ion-scale MHs in the solar wind are limited by measurement accuracy. Here, we present observations from Solar Orbiter (SolO) of an ion-scale MH embedded in the solar wind. The accurate and high-resolution measurements of ion velocity distributions allow us to investigate the detailed ion dynamics inside it.

2. Observations

The MH event was observed by the Solar Orbiter (SolO) spacecraft on 2 September 2020, at a heliocentric distance of 0.9 AU. The MH radius is estimated to be approximately 1,600 km ($\sim 13\rho_i$), identifying it as an ion-scale structure. Magnetic field measurements were provided by the onboard Magnetometer (MAG) (T. Horbury et al., 2020). Accurate ion moments and three-dimensional (3-D) velocity distribution functions (VDFs) were obtained from the Proton and Alpha particle Sensor (PAS) of the Solar Wind Analyzer (SWA) suite (Owen, Bruno, et al., 2020). Notably, during this event, SWA-PAS operated in burst mode with a high time resolution of 0.25s, offering a unique opportunity to investigate the self-consistency between the depressed magnetic field and ion dynamics. The high-resolution plasma number density is derived from the probe-to-spacecraft potential based on the current balance between photoelectron emission from the spacecraft surface and the ambient plasma electron current. Using reference density measurements, a fitting procedure is applied to establish an empirical relationship between the two, enabling the determination of high-resolution electron number density from the potential data acquired by the Radio and Plasma Waves (RPW) instrument (Y. Khotyaintsev et al., 2021; Maksimovic et al., 2020a).

$\boldsymbol{V}_{\nabla P}$ The in situ measurements are initially in the spacecraft reference frame (SRF), in which the x axis points from the spacecraft toward the Sun. The z axis aligns with the electric antenna (ANT1) of RPW, and the y axis follows the right-hand rule. The measured ion bulk velocity is stable before and after this event, confirming that this structure is convected by the background solar wind flow. Its velocity $\boldsymbol{v}_{back} = (-320, 17, -9)$ km/s in SRF coordinates, averaged from 19:34:00 to 19:34:05 UT, is used to transform the measurements to the solar wind (or magnetic hole) rest frame. Also, based on the $\boldsymbol{v}_{back}$ and the background magnetic field $\boldsymbol{B}_b$, we construct an MH coordinate system to facilitate the analysis. In this system, the Z axis is aligned with the direction of $\boldsymbol{B}_b$, which remains relatively constant throughout this event. The X axis is set opposite to the projection of $\boldsymbol{v}_{back}$ in the plane

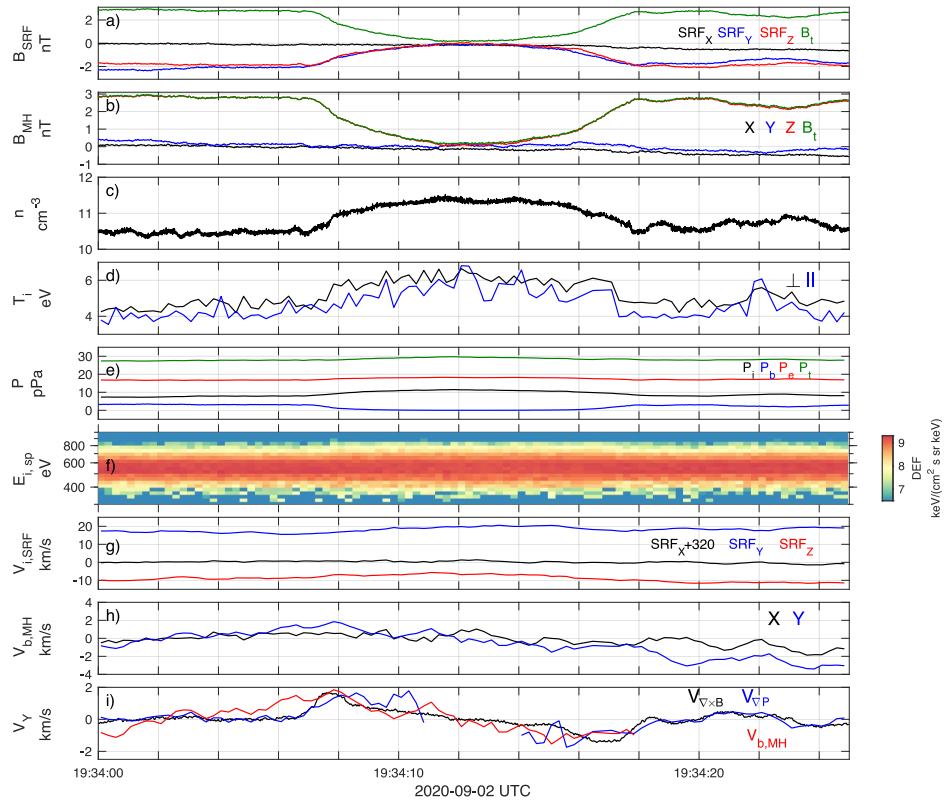

Figure 1. Solar Orbiter observations of an ion-scale magnetic hole. (a) Magnetic field in spacecraft reference frame. (b) Magnetic field in MH coordinate system. (c) Number density. (d) Ion perpendicular temperature (*black*) and parallel temperature (*blue*). (e) Pressures, including ion thermal pressure (P_i, *black*), magnetic pressure (P_b, *blue*), electron thermal pressure (P_e, *red*), and total pressure (P_t, *green*). (f) Ion energy fluxes in the spacecraft frame. (g) Ion bulk velocity in the spacecraft frame. (h) Perpendicular components of perturbed ion bulk velocity in MH coordinate system. (i) V_Y Components derived from the curvature of the magnetic field ($\boldsymbol{V}_{\nabla\times B}$, *black*), ion diamagnetic drift ($\boldsymbol{V}_{\nabla P}$, *blue*), and observations ($\boldsymbol{V}_{b,MH}$, *red*).

perpendicular to the Z axis, while the Y axis completes the right-handed triad. Therefore, the spacecraft traverses the MH along the positive X direction.

For measured VDFs in the spacecraft frame, we first transfer the corresponding ion velocity to the solar wind rest frame by subtracting $\boldsymbol{v}_{back}$, and then rotate it into MH coordinates to obtain $\boldsymbol{v}_{i,MH}$. This velocity is utilized throughout this study, unless otherwise specified. It allows us to define the particle energy E_{pl} in the plasma/solar wind frame, the pitch angle (PA, deviation between $\boldsymbol{v}_{i,MH}$ and Z axis), and the gyro-phase angle φ_v (the phase difference between the perpendicular component of $\boldsymbol{v}_{i,MH}$ and the X axis). Thus, the energy E_{pl} spectrum is given by the distributions averaged over both the PA and φ_v. The pitch angle spectrum is derived by averaging over φ_v for the distributions in a specific E_{pl} range. Finally, by restricting both the E_{pl} and PA ranges, we can compute the corresponding gyro-phase φ_v spectrum.

Figure 1 shows an overview of this event. The magnetic field measured in SRF coordinates (Figure 1a) is then transferred into the MH coordinate system (Figure 1b), revealing a pronounced depression with a minimum field strength of 0.15 nT. The total magnetic strength (B_t, green line) closely follows the B_Z component (red line), indicative of a linear MH in which the magnetic field direction varies only slightly, as opposed to strongly twisted or rotating configurations. This magnetic depression is accompanied by enhancements in both plasma number density and ion perpendicular temperature (Figures 1c and 1d). Consequently, the increase in ion and electron thermal plasma pressure ($P_i = n_e k T_{i,\perp}$, $P_e = n_e k T_e$, assuming $T_e = 10$ eV and $n_i = n_e$) compensates for the reduction in magnetic pressure P_b, leading to a quasi-constant total pressure ($P_t = P_b + P_i + P_e$) in Figure 1e. This pressure balance signature indicates a stable ion-scale MH in the solar wind, which is consistent with the quasi-symmetric properties in Figure 1. The increase in ion temperature is also evident from the slight broadening

of the ion energy spectrum in the spacecraft frame (Figure 1f), which becomes more pronounced after subsequent transformation to the plasma frame.

The ion-scale MH is likely associated with an ion vortex, which is usually assumed to have a circular cross-section in the plane perpendicular to the background magnetic field (Li, Zhou, Zong, et al., 2021; T. Zhang et al., 2008). To explore this property, we use the measured ion bulk velocity in Figure 1g to calculate its perturbations $\boldsymbol{V}_{b,MH} = V_X\boldsymbol{e}_X, V_Y\boldsymbol{e}_Y, V_Z\boldsymbol{e}_Z$ in the MH frame and coordinates, shown in Figure 1h. The observed bipolar signature of the V_Y component reflects an azimuthal ion flow, which is the characteristic feature for the ion vortex (Wang et al., 2021). Simultaneously, the V_X oscillates around zero (black dashed line), implying that the spacecraft traversed close to the MH center at T_c 19:34:12.4 UT (Li, Zhou, Yang, et al., 2021; Yao et al., 2023). To further examine the self-consistency of this structure, we organize its properties as functions of the distance between the spacecraft and the MH center $\rho = \delta t \cdot v_{bulk,X}$, which is determined based on the observed time difference δt from T_c and $v_{bulk,X}$, the X component of background solar wind velocity v_{back}.

At first, we apply Ampère's law, $\nabla \times \boldsymbol{B} = \mu_0 \boldsymbol{J}$, to estimate the ring current density $\boldsymbol{J}_{\nabla\times B}$ surrounding the MH. This corresponds to a velocity $\boldsymbol{V}_{\nabla\times B} = \boldsymbol{J}_{\nabla\times B}/(ne)$, which represents the theoretical velocity difference between the ions and electrons. Subsequently, we compute the ion diamagnetic drift velocity based on $\boldsymbol{V}_{\nabla P} = (\boldsymbol{B} \times \nabla P_i)/neB^2$ (Liu, Zong, Zhang, Xiao, et al., 2019; Yao et al., 2017). Thus, we could compare these calculated results with the observed V_Y in Figure 1i, which is not shown after 19:34:18 due to the perturbation by the second MH in Figure 1a at 19:34:22 UT. Meanwhile, $\boldsymbol{V}_{\nabla P}$ is absent at the center because ∇P_i carries large uncertainty, originating primarily from the determination of the MH center. Given that the MAG absolute calibration uncertainty ($\sim$0.1 nT) is comparable to the magnetic field minimum ($\sim$0.15 nT), the inferred center can shift slightly, which alters the distance ρ and, consequently, the estimate of ∇P_i. We note that the Y components of $\boldsymbol{V}_{\nabla P}$, $\boldsymbol{V}_{\nabla\times B}$ and $\boldsymbol{V}_{b,MH}$ are all close to each other, justifying the V_Y measurements with small deviations. This alignment supports the interpretation that the ion vortex generated by ion diamagnetic drift is consistent with the magnetic depression of MH. The minor deviation may stem from the calculation, the assumptions made, or the contribution from electrons.

Then, we investigate the detailed ion distributions in the solar wind frame. Figure 2a shows the ion energy spectrum of phase-space densities (PSDs), displaying enhancements inside the MH for tens of eV ions. To highlight variations inside and outside MH, we compute the normalized residual PSDs in Figure 2b. They are defined as $\hat{P} = \frac{P-\bar{P}}{\sigma_P}$, where $\bar{P}$ and σ_P represent the average and standard deviation of PSDs. This spectrum highlights a depletion of ions below 10 eV and a significant enhancement above 10 eV. Such a variation indicates that low-energy ions have been accelerated by the MH, resulting in an increase in temperature. Similar signatures have been observed for the electrons inside the sub-ion MH (Yao et al., 2017).

The pitch angle distributions of PSDs and residual PSDs for 20–100 eV ions are shown in Figures 2c and 2d. The pronounced PSD enhancement indicates that more ions are trapped within the MH. In addition to the contribution from increased number density, the enhancement spanning approximately 0°–180° in pitch angle is also consistent with simultaneous increases in both parallel and perpendicular ion temperatures (Figure 1d). The resulting quasi-isotropic ion distribution is further supported by the reduced 2-D velocity distribution in the X–Z plane (Figure 2h), which displays nearly circular PSD contours in the spacecraft frame. This quasi-isotropy is quantitatively confirmed by the eigenvalues of the temperature tensor (Richard et al., 2025), which are closely spaced: $\lambda_1 = 6.9, \lambda_2 = 6, \lambda_3 = 5.3$. The isotropic signature differs markedly from MMS observations of ion-scale MHs in the magnetosheath, which often exhibit strong temperature anisotropies (Ahmadi et al., 2018; Yao et al., 2019).

This discrepancy is possibly related to the width of the loss cone. The MHs are usually embedded within a mirror-mode wave environment, accompanied by a local loss cone defined by $\sin\alpha = \sqrt{B_t/B_{\max}}$ (see the black lines for α in Figures 2c and 2d), where $B_{\max}$ represents the maximum of magnetic strength along the field line. As B_t approaches zero, the loss cone at the center spans nearly 0° to 180°, indicating a significant trapping process. As a result, the synchronous trapping of perpendicular- and parallel-moving ions leads to the formation of quasi-isotropic ion distributions. In contrast, the shallow MH in the magnetosheath traps particles with pitch angles $\sim$90°, leading to the temperature anisotropy with $T_\perp > T_\parallel$.

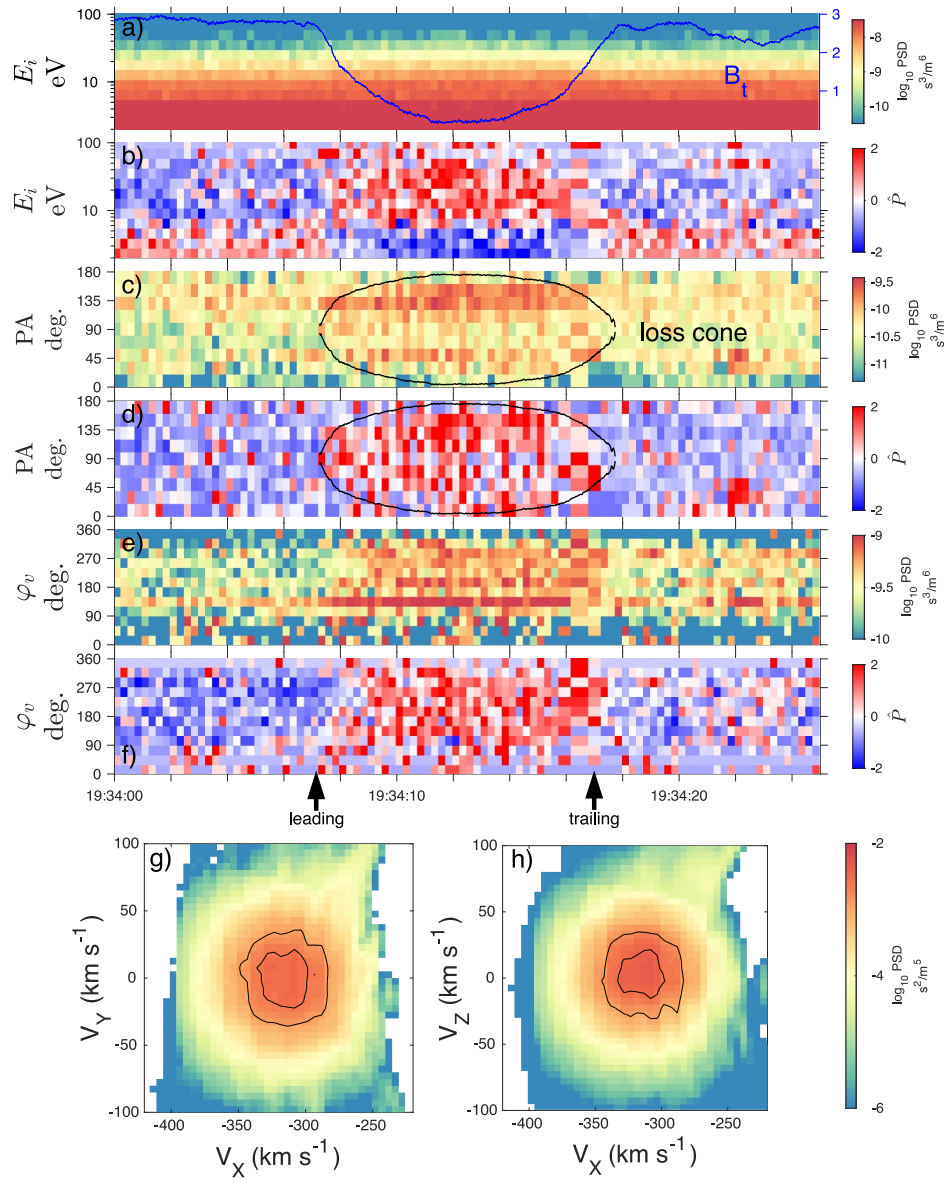

Figure 2. Observed ion distributions of phase-space densities (PSDs) and residual PSDs ($\hat{P}$). (a, b) Ion energy spectra of PSD and $\hat{P}$ in MH frame. The *blue* line represents the total magnetic field strength. (c, d) Ion pitch angle spectra of PSD and $\hat{P}$ in MH frame for 20–100 eV ions, averaged over the plane perpendicular to the background magnetic field. The *black* lines indicate the loss cone angles α, defined by $\sin\alpha = \sqrt{B_t/B_{\max}}$. (e, f) Ion gyro-phase spectra of PSD and $\hat{P}$ in MH frame, for 20–40 eV ions with pitch angles of $90^\circ \pm 40^\circ$. (g, h) Reduced 2-D distributions in the $X-Y$ and $X-Z$ planes and in the spacecraft frame. The *black* lines denote the PSD contours.

Figures 2e and 2f display the gyro-phase (φ_v) spectra of PSDs and residual PSDs for 20–40 eV ions with pitch angles between $90^\circ \pm 40^\circ$. The distributions are gyrotropic at the center (see Figure 2g), but become increasingly agyrotropic toward the boundaries. As seen from Figure 2f, enhanced PSDs are observed at $\varphi_v \sim 90^\circ$ at the leading boundary, in comparison with the peak $\varphi_v \sim 270^\circ$ at the trailing boundary. This agyrotropy aligns with the bipolar V_Y ion flow in Figure 1h, further demonstrating the presence of an ion vortex (Li et al., 2020).

The combined Solar Orbiter measurements of the magnetic field, ion moments, and VDFs provide a self-consistent characterization of the ion-scale MH in the solar wind, which can trap the protons and form the diamagnetic current to maintain the depressed magnetic field.

3. Model Results and Comparison With Observations

Solar Orbiter provides measurements along a single spacecraft trajectory, offering only a one-dimensional cut through the MH. A complete understanding of it, therefore, requires the application of kinetic models capable of reconstructing its full three-dimensional configuration. To achieve this aim, we apply a kinetic equilibrium model to reconstruct the observed MH (Li et al., 2020; Shustov et al., 2016).

This model is a self-consistent solution to the coupled Vlasov-Maxwell system in the cylindrical coordinates (ρ, φ, z). The magnetic field $\boldsymbol{B}$ possesses only a $B_z\boldsymbol{e}_z$ component, which is determined by the magnetic vector potential $\boldsymbol{A} = A_\varphi(\rho)\boldsymbol{e}_\varphi$. The electric field $\boldsymbol{E}$ is derived from the electric scalar potential $\phi(\rho)$. To describe corresponding particle distributions, we introduce two invariants. One is the particle energy $H_\alpha = \frac{1}{2m_\alpha}\left(\boldsymbol{P} - q_\alpha \boldsymbol{A}\right)^2 + q_\alpha\phi$, where $\boldsymbol{P}$ represents the canonical momentum. Here, $\alpha = e, i$ denotes electrons and ions, respectively. Since H_α is independent of the azimuthal coordinate φ, the canonical angular momentum $P_{\varphi\alpha} = \rho\left(M_\alpha v_\varphi + q_\alpha A_\varphi\right)$ (azimuthal component of $\boldsymbol{P}$) is also conserved (Li et al., 2020). Utilizing these two invariants H_α and $P_{\varphi\alpha}$, we construct the electron/ion VDF,

$$f_\alpha = \delta N\left(\frac{M_\alpha}{2\pi\theta_{\alpha,0}}\right)^{\frac{3}{2}} \exp\left(-\frac{H_\alpha}{\theta_{\alpha,0}}\right) + (1-\delta)N\left(\frac{M_\alpha}{2\pi\theta_{\alpha,1}}\right)^{\frac{3}{2}} \exp\left(-\frac{H_\alpha - \Omega_\alpha P_{\varphi\alpha}}{\theta_{\alpha,1}}\right), \quad (1)$$

which naturally satisfies the Vlasov equation.

The ion/electron distribution consists of a Maxwellian background population (denoted by subscript 0) and a shifted-Maxwellian current-carrying population (denoted by subscript 1) (Yao et al., 2023). Some model parameters are directly obtained based on the observations, such as the total ion number density N =11.3 cm^{-3}, background ion temperature $\theta_{i,0} = 4.5$ eV, and electron temperature $\theta_{e,0} = \theta_{e,1} = 10$ eV. Assuming the background ion population accounts for 93% ($\delta = 0.93$) of the total ion density, the observed $T_i = 5.7$ eV at the MH center is actually a weighted average of $\theta_{i,0}$ and $\theta_{i,1}$, consistent with $\theta_{i,1} = 22.6$ eV for the current-carrying population. Subsequently, we adjust the angular velocities of the current-carrying populations to best match the model with the spacecraft observations, setting $\Omega_i = -0.013$ s^{-1} for ions and $\Omega_e = 0.0013$ s^{-1} for electrons, respectively. Thus, we can integrate the ion/electron VDF to derive profiles of number density and bulk velocity, which are then substituted into Maxwell's equations to obtain self-consistent electromagnetic fields.

Figure 3 presents the virtual spacecraft observations of the modeled MH as solid lines. Based on the ρ derived above, we can correspondingly extract model properties along the path of the SolO. The top three panels show that the magnetic field depression is accompanied by enhancements in ion number density and temperature. The total pressure, comprising magnetic, ion thermal, and electron thermal contributions, remains constant throughout the structure (Figure 3d). As for the bulk velocity, the bipolar V_Y in Figure 3e confirms the presence of an ion vortex. For comparison, we overplot the in situ Solar Orbiter observations as dashed lines in Figures 3a–3e, which exhibit great agreement with the model predictions.

The bottom three panels display the modeled ion energy, pitch angle, and gyro-phase spectra of PSDs, which are in the same format as the corresponding observations in Figure 2. The energy spectrum in Figure 3f reveals a clear PSD enhancement for ions above 10 eV. These energized ions are trapped across all pitch angles around the MH center (Figure 3g). Adjacent to the boundaries, strong agyrotropy appears in Figure 3h, which is associated with the ion azimuthal drift in the perpendicular plane (Figure 3e). Collectively, the signatures for the observed MH are well reproduced by the kinetic equilibrium model, demonstrating the self-consistency and stability of ion-scale MH in the solar wind.

4. Discussions

We have investigated an ion-scale MH event in the solar wind with detailed ion distribution measurements. This MH exhibits quasi-isotropic ion distributions at its center, in contrast to the typically anisotropic distributions in the solar wind. The observations also differ from the pancake pitch angle distributions reported inside magnetosheath MHs, suggesting that MHs follow distinct evolutionary pathways in different plasma environments (Li et al., 2020). The discrepancy is possibly associated with the deep MH, which has a large loss cone spanning from 0° to 180° in this event, leading to significant trapping. As the magnetic field strength approaches zero,

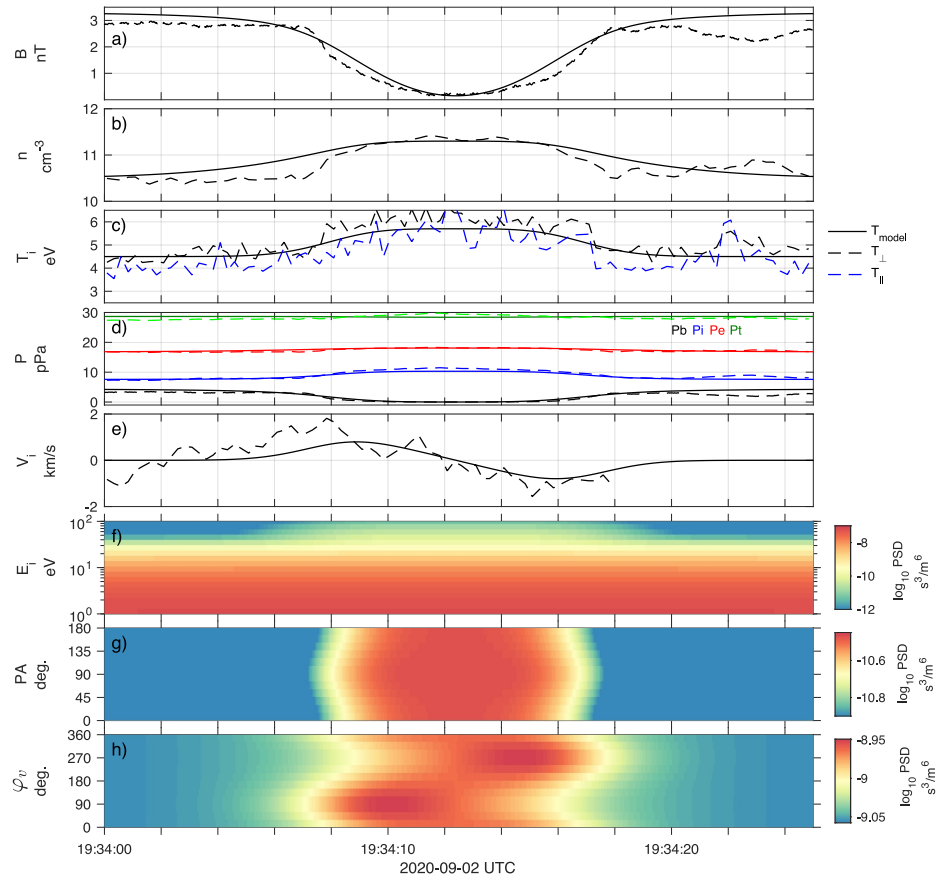

Figure 3. Comparison between model results and solar orbiter observations. The *solid* lines denote the virtual spacecraft observations, while the actual observations are shown as *dashed* lines. (a) Magnetic field. (b) Number density. (c) Temperatures, including the modeled ion temperature (*black solid* line) and observed ion perpendicular (*black dashed* line) and parallel temperatures (*blue dashed* line). (d) Pressures, including magnetic pressure (P_b, *black*), ion thermal pressure (P_i, *blue*), electron thermal pressure (P_e, *red*), and total pressure (P_t, *green*). (e) *Y* Component of ion bulk velocity. (f–h) Modeled ion energy, pitch angle, and gyro-phase spectra of phase-space densities in the same format as Figure 2.

particles become largely decoupled from magnetic control and tend toward an unmagnetized state, a regime of particular interest for investigating formation and evolutionary processes. Another possible mechanism is the field line scattering process, which can also contribute to the quasi-isotropic distribution (Richard et al., 2023). In this event, the ion gyroradius at the MH center exceeds the spatial scale of the structure, so the ions experience strong magnetic field gradients during gyration, which perturbs their magnetic moments (Treumann et al., 2004). Additionally, the deviation between the parallel magnetic field component B_Z and the total magnetic field strength B_t (see Figure 1b) and the measurement uncertainties indicate an abrupt change in magnetic field direction near the MH center, leading to possible scattering by the field curvature (Büchner & Zelenyi, 1989; Richard et al., 2023). Thus, the trapping and scattering effects can both contribute to the observed isotropic and gyrotropic ion distributions, but distinguishing their corresponding contributions requires multi-spacecraft observations. Notably, in both mechanisms, the extremely low magnetic field of 0.15 nT plays a crucial role in significantly affecting ion dynamics. Therefore, understanding how such a deep magnetic depression forms and what determines the evolutionary paths in different environments are important directions in the future.

The ion energy spectrum indicates that the temperature increase arises from accelerating ions with energies below 10 eV up to around 100 eV. This acceleration may be related to the MH formation and evolution processes. In situ observations have demonstrated the shrinking evolution of sub-ion MHs (Liu, Zong, Zhang, Sun, et al., 2019), which are accompanied by the azimuthal electric fields. As the electron gyroradius becomes comparable to the structure size, electrons can be accelerated during their gyromotion by the shrinking sub-ion MH (Liu

et al., 2020). By analogy, electric fields within ion-scale MHs may be critical to impacting ion dynamics, although further detailed observations and simulations are necessary to confirm this.

Ion-scale MHs may also influence energy dissipation at electron scales. In the terrestrial magnetosheath, electrons are preferentially heated in the perpendicular directions, forming an anisotropic distribution and thereby exciting whistler waves (Kitamura et al., 2020; Yao et al., 2019). In contrast, Solar Orbiter observations reveal a high occurrence rate of Langmuir waves inside ion-scale MHs in the solar wind, indicating an interaction with strahl electrons (Boldú et al., 2023; Briand et al., 2010; Liu et al., 2025). Thus, the ion-scale MHs in different plasma environments can impact distinct electron populations. On the other hand, since the electron temperature is generally greater than the ion temperature in the solar wind, electron thermal pressure makes a significant contribution to the total pressure. Therefore, the electron distribution is critical for the stability of ion-scale MHs in the solar wind.

5. Conclusion

In summary, we use Solar Orbiter observations to investigate ion dynamics within an ion-scale MH in the solar wind. We find that the MH is accompanied by an ion vortex, which is generated by the ion diamagnetic drift and drives the agyrotropy appearing at the MH boundaries. Notably, we observe energized ions inside the MH, as evidenced by significant PSD enhancements for the ions with energies exceeding 10 eV in the solar wind frame. As the magnetic field strength diminishes toward zero, the ion temperatures are increased simultaneously in both perpendicular and parallel directions, generating quasi-isotropic distributions. Subsequently, we employ a kinetic equilibrium model to reconstruct the MH, which matches well with the actual observations, supporting the interpretation that ion-scale MHs are self-consistent, stable structures in the solar wind. The agreement between the equilibrium model and observations explains why these ion-scale structures can be widely observed in the solar wind. Moreover, this self-consistent model provides a useful framework for future investigations of the formation mechanisms, evolutionary processes, and connections to ion energization.

Conflict of Interest

The authors declare no conflicts of interest relevant to this study.

Data Availability Statement

Solar Orbiter data are available at http://soar.esac.esa.int/soar/. The data from MAG (T. S. Horbury, et al., 2020), SWA (Owen, Nicolaou, et al., 2020), and RPW (Maksimovic et al., 2020b) instruments are used in this research. The data are processed and analyzed using the IRFU-Matlab package (Y. V. Khotyaintsev et al., 2022). The model results are deposited in Li (2025).

Acknowledgments
This work was supported by the Swedish Research Council Grant 2023-05048 and SNSA Grant 2023-00259. Solar Orbiter magnetometer operations are funded by the UK Space Agency (Grant UKRI943). Tim Horbury is supported by STFC Grant ST/W001071/1. We are grateful to the Solar Orbiter mission for the high-resolution measurements.

References

Ahmadi, N., Wilder, F. D., Ergun, R., Argall, M., Usanova, M., Breuillard, H., et al. (2018). Generation of electron whistler waves at the mirror mode magnetic holes: MMS observations and PIC simulation. *Journal of Geophysical Research: Space Physics*, *123*(8), 6383–6393. https://doi.org/10.1029/2018ja025452

Boldú, J., Graham, D., Morooka, M., André, M., Khotyaintsev, Y. V., Karlsson, T., et al. (2023). Langmuir waves associated with magnetic holes in the solar wind. *Astronomy & Astrophysics*, *674*, A220. https://doi.org/10.1051/0004-6361/202346100

Briand, C., Soucek, J., Henri, P., & Mangeney, A. (2010). Waves at the electron plasma frequency associated with solar wind magnetic holes: STEREO/Cluster observations. *Journal of Geophysical Research*, *115*(A12), A12113. https://doi.org/10.1029/2010ja015849

Büchner, J., & Zelenyi, L. M. (1989). Regular and chaotic charged particle motion in magnetotaillike field reversals: 1. Basic theory of trapped motion. *Journal of Geophysical Research*, *94*(A9), 11821–11842. https://doi.org/10.1029/ja094ia09p11821

Cattaneo, M. B., Basile, C., Moreno, G., & Richardson, J. (1998). Evolution of mirror structures in the magnetosheath of Saturn from the bow shock to the magnetopause. *Journal of Geophysical Research*, *103*(A6), 11961–11972. https://doi.org/10.1029/97ja03683

Dimmock, A. P., Yordanova, E., Graham, D. B., Khotyaintsev, Y. V., Blanco-Cano, X., Kajdič, P., et al. (2022). Mirror mode storms observed by Solar Orbiter. *Journal of Geophysical Research: Space Physics*, *127*(11), e2022JA030754. https://doi.org/10.1029/2022ja030754

Goodrich, K. A., Bonnell, J. W., Curry, S., Livi, R., Whittlesey, P., Mozer, F., et al. (2021). Evidence of subproton-scale magnetic holes in the Venusian magnetosheath. *Geophysical Research Letters*, *48*(5), e2020GL090329. https://doi.org/10.1029/2020gl090329

Goodrich, K. A., Ergun, R. E., & Stawarz, J. E. (2016). Electric fields associated with small-scale magnetic holes in the plasma sheet: Evidence for electron currents. *Geophysical Research Letters*, *43*(12), 6044–6050. https://doi.org/10.1002/2016gl069601

Haynes, C. T., Burgess, D., Camporeale, E., & Sundberg, T. (2015). Electron vortex magnetic holes: A nonlinear coherent plasma structure. *Physics of Plasmas*, *22*(1), 012309. https://doi.org/10.1063/1.4906356

Horbury, T., O'brien, H., Blazquez, I. C., Bendyk, M., Brown, P., Hudson, R., et al. (2020). The solar orbiter magnetometer. *Astronomy & Astrophysics*, *642*, A9. https://doi.org/10.1051/0004-6361/201937257

Horbury, T. S., de Witt, T. D., Zouganelis, I., St. Cyr, O. C., Kretzschmar, M., & other members of the Solar Orbiter MAG team. (2020). MAG instrument, Solar Orbiter Level 2 data [Dataset]. *European Space Agency Data Archive*. https://doi.org/10.5270/esa-ux7y320

Huang, S., Lin, R., Yuan, Z., Jiang, K., Wei, Y., Xu, S., et al. (2021). In situ detection of kinetic-size magnetic holes in the Martian magnetosheath. *The Astrophysical Journal*, *922*(2), 107. https://doi.org/10.3847/1538-4357/ac2737

Huang, S., Wei, Y., Zhao, J., Yuan, Z., Deng, X., Jiang, K., et al. (2022). Kinetic-size magnetic holes in the terrestrial foreshock region. *Geophysical Research Letters*, *49*(8), e2021GL093813. https://doi.org/10.1029/2021gl093813

Joy, S., Kivelson, M., Walker, R., Khurana, K., Russell, C., & Paterson, W. (2006). Mirror mode structures in the Jovian magnetosheath. *Journal of Geophysical Research*, *111*(A12), A12212. https://doi.org/10.1029/2006ja011985

Karlsson, T., Trollvik, H., Raptis, S., Nilsson, H., & Madanian, H. (2022). Solar wind magnetic holes can cross the bow shock and enter the magnetosheath. *Annales Geophysicae*, *40*(6), 687–699. https://doi.org/10.5194/angeo-40-687-2022

Khotyaintsev, Y., Vaivads, A., Johansson, E. P. G., Nilsson, T., Karlsson, J., Graham, D., & Lindberg, M. (2022). irfu/irfu-matlab: V1.16.3, [Software]. *Zenodo*. https://doi.org/10.5281/zenodo.11550091

Khotyaintsev, Y. V., Graham, D. B., Vaivads, A., Steinvall, K., Edberg, N. J., Eriksson, A. I., et al. (2021). Density fluctuations associated with turbulence and waves-first observations by solar orbiter. *Astronomy & Astrophysics*, *656*, A19. https://doi.org/10.1051/0004-6361/202140936

Kitamura, N., Omura, Y., Nakamura, S., Amano, T., Boardsen, S., Ahmadi, N., et al. (2020). Observations of the source region of whistler mode waves in magnetosheath mirror structures. *Journal of Geophysical Research: Space Physics*, *125*(5), e2019JA027488. https://doi.org/10.1029/2019ja027488

Li, J.-H. (2025). Solar orbiter observations of a self-consistent ion-scale magnetic hole at 0.9AU [Software]. *Zenodo*. https://doi.org/10.5281/zenodo.17376561

Li, J.-H., Yang, F., Zhou, X.-Z., Zong, Q.-G., Artemyev, A. V., Rankin, R., et al. (2020). Self-consistent kinetic model of nested electron-and ion-scale magnetic cavities in space plasmas. *Nature Communications*, *11*(1), 5616. https://doi.org/10.1038/s41467-020-19442-0

Li, J.-H., Zhou, X.-Z., Yang, F., Artemyev, A. V., & Zong, Q.-G. (2021). Helical magnetic cavities: Kinetic model and comparison with Mms observations. *Geophysical Research Letters*, *48*(6), e2021GL092383. https://doi.org/10.1029/2021gl092383

Li, J.-H., Zhou, X.-Z., Zong, Q.-G., Yang, F., Fu, S., Yao, S., & Shi, Q. (2021). On the origin of donut-shaped electron distributions within magnetic cavities. *Geophysical Research Letters*, *48*(2), e2020GL091613. https://doi.org/10.1029/2020gl091613

Liu, C., Fu, H., Liu, Y., & Xu, Y. (2021). Kinetics of magnetic hole behind dipolarization front. *Geophysical Research Letters*, *48*(10), e2021GL093174. https://doi.org/10.1029/2021gl093174

Liu, H., Zong, Q.-G., Zhang, H., Sun, W., Zhou, X.-Z., Gershman, D. J., et al. (2019). The geometry of an electron scale magnetic cavity in the plasma sheet. *Geophysical Research Letters*, *46*(16), 9308–9317. https://doi.org/10.1029/2019gl083569

Liu, H., Zong, Q.-G., Zhang, H., Xiao, C., Shi, Q., Yao, S., et al. (2019). MMS observations of electron scale magnetic cavity embedded in proton scale magnetic cavity. *Nature Communications*, *10*(1), 1040. https://doi.org/10.1038/s41467-019-08971-y

Liu, J., Verscharen, D., Coburn, J., Nicolaou, G., Wu, X., Jiang, W., et al. (2025). Langmuir wave excitation in solar-wind magnetic holes. arXiv preprint arXiv:2507.02042. https://arxiv.org/abs/2507.02042

Liu, J., Yao, S., Shi, Q., Wang, X., Zong, Q., Feng, Y., et al. (2020). Electron energization and energy dissipation in microscale electromagnetic environments. *The Astrophysical Journal Letters*, *899*(2), L31. https://doi.org/10.3847/2041-8213/abab92

Maksimovic, M., Bale, S., Chust, T., Khotyaintsev, Y., Krasnoselskikh, V., Kretzschmar, M., et al. (2020a). The solar orbiter radio and plasma waves (RPW) instrument. *Astronomy & Astrophysics*, *642*, A12. https://doi.org/10.1051/0004-6361/201936214

Maksimovic, M., Bale, S. D., Chust, T., Khotyaintsev, Y. V., Krasnoselskikh, V., Kretzschmar, M., et al. (2020b). RPW—Radio and plasma waves instrument, solar orbiter level 2 data [Dataset]. *European Space Agency Data Archive*. https://doi.org/10.57780/esa-3xcjd4w

Owen, C. J., Bruno, R., Livi, S., Louarn, P., Al Janabi, K., Allegrini, F., et al. (2020). The solar orbiter solar wind analyser (SWA) suite. *Astronomy & Astrophysics*, *642*, A16. https://doi.org/10.1051/0004-6361/201937259

Owen, C. J., Nicolaou, G., Lewis, G., Razavi, A., & Maximovic, M., & other members of the UCL-IRF-ASI-SWRI SWA Consortium. (2020). SWA—Solar wind analyser suite, solar orbiter level 2 data [Dataset]. *European Space Agency Data Archive*. https://doi.org/10.5270/esa-ahypgn6

Plaschke, F., Karlsson, T., Goetz, C., Moestl, C., Richter, I., Volwerk, M., et al. (2018). First observations of magnetic holes deep within the coma of a comet. *Astronomy & Astrophysics*, *618*, A114. https://doi.org/10.1051/0004-6361/201833300

Richard, L., Khotyaintsev, Y. V., Graham, D. B., Vaivads, A., Gershman, D. J., & Russell, C. T. (2023). Fast ion isotropization by current sheet scattering in magnetic reconnection jets. *Physical Review Letters*, *131*(11), 115201. https://doi.org/10.1103/physrevlett.131.115201

Richard, L., Servidio, S., Svenningsson, I., Artemyev, A. V., Klein, K. G., Yordanova, E., et al. (2025). Non-Maxwellianity of ion velocity distributions in the Earth's magnetosheath. arXiv preprint arXiv:2504.05502. *Physical Review*, *112*(5), L053201. https://doi.org/10.1103/7p1x-84y9

Roberts, O., Nakamura, R., Coffey, V., Gershman, D., Volwerk, M., Varsani, A., et al. (2021). A study of the solar wind ion and electron measurements from the magnetospheric multiscale mission's fast plasma investigation. *Journal of Geophysical Research: Space Physics*, *126*(10), e2021JA029784. https://doi.org/10.1029/2021ja029784

Russell, C., Jian, L., Luhmann, J., Zhang, T., Neubauer, F., Skoug, R. M., et al. (2008). Mirror mode waves: Messengers from the coronal heating region. *Geophysical Research Letters*, *35*(15), L15101. https://doi.org/10.1029/2008gl034096

Russell, C., Riedler, W., Schwingenschuh, K., & Yeroshenko, Y. (1987). Mirror instability in the magnetosphere of comet Halley. *Geophysical Research Letters*, *14*(6), 644–647. https://doi.org/10.1029/gl014i006p00644

Shi, Q., Yao, S., Hamrin, M., & Liu, J. (2024). Kinetic scale magnetic holes in the terrestrial magnetosheath: A review. *Science China Earth Sciences*, *67*(9), 2739–2771. https://doi.org/10.1007/s11430-023-1290-8

Shustov, P., Artemyev, A., Vasko, I., & Yushkov, E. (2016). Kinetic models of sub-ion cylindrical magnetic hole. *Physics of Plasmas*, *23*(12), 122903. https://doi.org/10.1063/1.4972093

Sperveslage, K., Neubauer, F., Baumgärtel, K., & Ness, N. (2000). Magnetic holes in the solar wind between 0.3 AU and 17 AU. *Nonlinear Processes in Geophysics*, *7*(3/4), 191–200. https://doi.org/10.5194/npg-7-191-2000

Treumann, R. A., Jaroschek, C. H., Constantinescu, O. D., Nakamura, R., Pokhotelov, O. A., & Georgescu, E. (2004). The strange physics of low frequency mirror mode turbulence in the high temperature plasma of the magnetosheath. *Nonlinear Processes in Geophysics*, *11*(5/6), 647–657. https://doi.org/10.5194/npg-11-647-2004

Trollvik, H., Karlsson, T., & Raptis, S. (2023). Velocity of magnetic holes in the solar wind from Cluster multipoint measurements. *Annales Geophysicae Discussions*, *2023*(2), 1–15. https://doi.org/10.5194/angeo-41-327-2023

Turner, J., Burlaga, L., Ness, N., & Lemaire, J. (1977). Magnetic holes in the solar wind. *Journal of Geophysical Research*, *82*(13), 1921–1924. https://doi.org/10.1029/ja082i013p01921

Wang, G., Volwerk, M., Wu, M., Hao, Y., Xiao, S., Wang, G., et al. (2021). First observations of an ion vortex in a magnetic hole in the solar wind by MMS. *The Astronomical Journal*, *161*(3), 110. https://doi.org/10.3847/1538-3881/abd632

Wang, G., Volwerk, M., Xiao, S., Wu, M., Chen, Y., & Zhang, T. (2022). Electron-scale current sheet as the boundary of a linear magnetic hole in the terrestrial current sheet observed by the magnetospheric multiscale mission. *Journal of Geophysical Research: Space Physics*, *127*(5), e2021JA029707. https://doi.org/10.1029/2021ja029707

Wang, S., Wang, R., Lu, Q., Lu, S., & Huang, K. (2024). Direct observation of magnetic reconnection resulting from interaction between magnetic flux rope and magnetic hole in the Earth's magnetosheath. *Geophysical Research Letters*, *51*(12), e2023GL107968. https://doi.org/10.1029/2023gl107968

Wilson, L. B., III., Goodrich, K. A., Turner, D. L., Cohen, I. J., Whittlesey, P. L., & Schwartz, S. J. (2022). The need for accurate measurements of thermal velocity distribution functions in the solar wind. *Frontiers in Astronomy and Space Sciences*, *9*, 1063841. https://doi.org/10.3389/fspas.2022.1063841

Winterhalter, D., Neugebauer, M., Goldstein, B. E., Smith, E. J., Bame, S. J., & Balogh, A. (1994). Ulysses field and plasma observations of magnetic holes in the solar wind and their relation to mirror-mode structures. *Journal of Geophysical Research*, *99*(A12), 23371–23381. https://doi.org/10.1029/94ja01977

Xiao, T., Shi, Q., Zhang, T., Fu, S., Li, L., Zong, Q., et al. (2010). Cluster-C1 observations on the geometrical structure of linear magnetic holes in the solar wind at 1 AU. *Annales Geophysicae*, *28*(9), 1695–1702. https://doi.org/10.5194/angeo-28-1695-2010

Yao, S., Li, J., Zhou, X.-Z., Shi, Q., Zong, Q.-G., Zhang, H., et al. (2023). Ion-vortex magnetic hole with reversed field direction in Earth's magnetosheath. *Journal of Geophysical Research: Space Physics*, *128*(7), e2023JA031749. https://doi.org/10.1029/2023ja031749

Yao, S., Shi, Q., Li, Z., Wang, X., Tian, A., Sun, W., et al. (2016). Propagation of small size magnetic holes in the magnetospheric plasma sheet. *Journal of Geophysical Research: Space Physics*, *121*(6), 5510–5519. https://doi.org/10.1002/2016ja022741

Yao, S., Shi, Q., Liu, J., Yao, Z., Guo, R., Ahmadi, N., et al. (2018). Electron dynamics in magnetosheath mirror-mode structures. *Journal of Geophysical Research: Space Physics*, *123*(7), 5561–5570. https://doi.org/10.1029/2018ja025607

Yao, S., Shi, Q., Yao, Z., Li, J., Yue, C., Tao, X., et al. (2019). Waves in kinetic-scale magnetic dips: MMS observations in the magnetosheath. *Geophysical Research Letters*, *46*(2), 523–533. https://doi.org/10.1029/2018gl080696

Yao, S., Wang, X., Shi, Q., Pitkänen, T., Hamrin, M., Yao, Z., et al. (2017). Observations of kinetic-size magnetic holes in the magnetosheath. *Journal of Geophysical Research: Space Physics*, *122*(2), 1990–2000. https://doi.org/10.1002/2016ja023858

Yao, S., Yue, Z., Shi, Q., Degeling, A. W., Fu, H., Tian, A., et al. (2021). Statistical properties of kinetic-scale magnetic holes in terrestrial space. *Earth and Planetary Physics*, *5*(1), 63–72. https://doi.org/10.26464/epp2021011

Yao, S., Zhang, H., Shi, Q., Liu, J., Guo, R., Sun, W., et al. (2024). Electron vortex generation in Earth's collisionless bow shock: MMS observations. *Journal of Geophysical Research: Space Physics*, *129*(9), e2024JA032980. https://doi.org/10.1029/2024ja032980

Yu, L., Huang, S., Yuan, Z., Jiang, K., Xiong, Q., Xu, S., et al. (2021). Characteristics of magnetic holes in the solar wind revealed by parker solar probe. *The Astrophysical Journal*, *908*(1), 56. https://doi.org/10.3847/1538-4357/abb9a8

Zhang, T., Russell, C., Baumjohann, W., Jian, L., Balikhin, M., Cao, J., et al. (2008). Characteristic size and shape of the mirror mode structures in the solar wind at 0.72 AU. *Geophysical Research Letters*, *35*(10), L10106. https://doi.org/10.1029/2008gl033793

Zhang, X.-J., Artemyev, A., Angelopoulos, V., & Horne, R. (2017). Kinetics of sub-ion scale magnetic holes in the near-Earth plasma sheet. *Journal of Geophysical Research: Space Physics*, *122*(10), 10–304. https://doi.org/10.1002/2017ja024197